Surface-Enhanced Raman Scattering Studies on Aggregated Silver Nanoplates in Aqueous Solution

Xiangqin Zou and Shaojun Dong*

State Key Laboratory of Electroanalytic Chemistry, Changchun Institute of Applied Chemistry, Graduate School, Chinese Academy of Sciences, Changchun, Jilin 130022, China

Received: June 11, 2006; In Final Form: August 4, 2006

Four different sizes of citrate-protected silver nanoplates with the corresponding in-plane dipole resonance band at 530, 619, 778, and 858 nm, respectively, are synthesized for surface-enhanced Raman scattering (SERS) study. Their aggregation behaviors are monitored by use of UV−vis spectroscopy. During the aggregation process, a marked red shift of the in-plane dipole resonance of silver nanoplates is observed, whereas other resonance modes of them only have small alterations in the site or intensity. Aggregated silver nanoplates can serve as active SERS substrates with an enhancement factor of about 4.5×10^5 using 2-aminothiophenol as a probing molecule. The SERS performance of silver nanoplates is even superior to the commonly used Lee−Meisel silver colloid, making them very attractive for SERS applications.

Introduction

Metal colloids have been widely employed in surface-enhanced Raman spectroscopy (SERS) because they have a number of advantages, such as ease of formation and manipulation, ability to control and vary particle size and shape, and a more tractable morphology for theoretical analysis, etc.[1] Up to now, the most frequently used silver colloids for SERS measurements are produced by reduction of silver nitrate with sodium citrate.[2−4] Other reducing methods including borohydride,[5] hydrazine,[6] hydroxylamine,[7,8] and hydrogen peroxide[9] were also developed for preparing SERS-active silver colloids. But all the obtained colloids were basically nearly spherical, whereas less attention was paid to platelike ones.

Silver nanoplates were highly oriented single crystals with (111) planes as the basal plane. The sides or edges of nanoplates were mainly bound by (110) or (100) planes.[10d] Because of high anisotropy in their dimensions, the optical properties of silver nanoplates are more rich and complicated than those of normal spherical nanoparticles.[10] As calculated by Jin et al.,[10a] the SPR absorption spectra of perfect silver nanoprisms show a weak transversal out-of-plane (410 nm) dipole band and a very intense in-plane (770 nm) dipole band, the weak in-plane (470 nm) and out-of-plane (340 nm) quadrupole resonance. Recent discrete dipole approximation (DDA) investigations[11] also showed that the real optical properties of silver nanoplates were related to their size, snip, aspect ratio, and environment. Unlike the normal spherical silver particles with a surface plasmon resonance (SPR) peak at ca. 420 nm,[2] the strong SPR peak of in-plane dipole resonance of silver nanoplates can be easily tuned from the visible to the near-IR region of the spectrum. These special morphologies and rich optical properties are expected to endow silver nanoplates with the SERS effectiveness different from other shaped silver colloids.

In this report, we studied the SERS activity of aggregated silver nanoplates in aqueous solution. The aggregated behaviors of them were monitored by UV−vis spectroscopy, and their SERS efficiency was tested using 2-aminothiophenol (2-ATP) as a probing molecule. Results showed aggregated silver nanoplates could be used as an active SERS substrate.

Experimental Section

Materials. $NaBH_4$ (98%) and 2-ATP were from Acros. The following analytical grade chemicals were purchased from domestic sources and used without further purification: $AgNO_3$, hydrated hydrazine, NaCl, and trisodium citrate. Milli-Q grade water (>18 MΩ) was used for all solution preparation and experiments.

Instrumentation. Samples for transmission electron microscopy (TEM) images were examined using a JEOL 2010 TEM operated at 200 KV. To analyze the samples by TEM, 1 mL of samples S1−S4 was purified by centrifugation. The upper part of the colorless solution was removed, and the solid portion was redispersed in 1 mL of pure water. A 5 μL aliquot of each purified sample was placed on a carbon-coated copper grid and allowed to dry in air. For each sample, usually over 200 particles from different parts of the grid were used to estimate the mean diameter and size distribution of particles. Optical spectra were acquired on a Cary 500 near-IR−UV−vis spectrophotometer using 1 cm light path quartz cuvette. Power X-ray diffraction (XRD) measurements were performed on Rigaku D/max 2000 X-ray diffractometer using Cu Kα radiation. SERS spectra using the excitation wavelength of 514.5 nm were measured with a renishaw 1000 model confocal microscopy Raman spectrometer. Fourier transform (FT) SERS spectra (the excitation wavelength was 1064 nm) were recorded on a Bruker IFS 66 FT-IR spectrometer. The laser power used was about 500 mW. The resolution of the Raman instrument was 4 cm^{-1}. All FT-Raman were recorded by averaging 512 scans.

Syntheses of Silver Nanoplates. Silver nanoplates were synthesized according to a modified procedure developed by our group. First, silver seeds were synthesized as follows: 0.5 mL of 59 mM $AgNO_3$ and 1 mL of 34 mM sodium citrate were added to 98 mL of aqueous solution. The solution was stirred for several minutes. Then, 0.5 mL of an aqueous 0.02 M $NaBH_4$

* Corresponding author. Fax: +86-431-5689711. E-mail: dongsj@ciac.jl.cn.

10.1021/jp063630h CCC: $33.50
Published on Web 10/04/2006

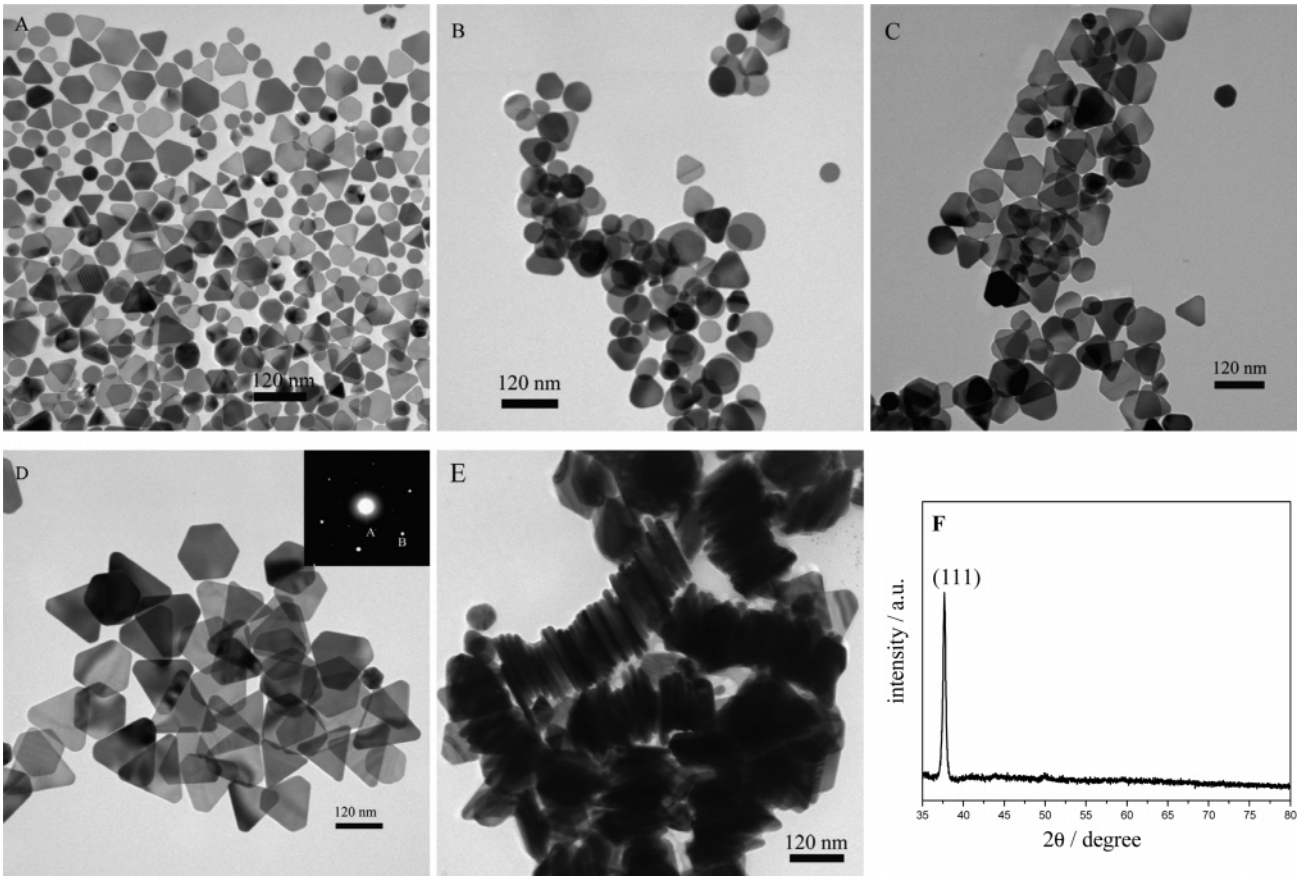

Figure 1. TEM images of (A) sample S1, (B) sample S2, (C) sample S3, and (D) sample S4. The inset shows a typical SAED pattern taken from an individual nanoplate. The strongest spots (letter B in the inset) could be indexed to the allowed {220} reflection, and the inner spots (letter A in the inset) with a weaker intensity corresponded to the formally forbidden (1/3){422} reflection. (E) Silver nanoplates stacking from sample S4. Statistical evaluation on the staking generated a thickness of ca. 14 nm for the silver nanoplates. (F) XRD pattern from sample S4.

solution, which had been aged for 2 h, was added all at once. The resultant solution was stirred for 1 h and aged for at least 24 h at room temperature before use. From TEM measurements, the silver seeds were nearly spherical with the diameter of 8.5 ± 3.5 nm and one SPR band at 392 nm. Then, silver nanoplates were prepared by enlarging these small silver seeds in the presence of citrate. Typically, two sets of solutions (1 and 2) were prepared. Solution 1 was prepared by injecting 900 μL of aqueous 40 mM hydrated hydrazine, 300 μL of aqueous 40 mM trisodium citrate, and different amounts of silver seeds to a 60 mL aqueous solution. Solution 2 was prepared by adding 300 μL of aqueous 59 mM $AgNO_3$ into 30 mL of aqueous solution. Then solution 2 was dropwise (1 mL/min) added into solution 1 under strong stirring. After the addition of solution 2 to 1 was finished, stirring was continued for 30 min. Four samples (S1−S4) were prepared with 2000, 700, 400, and 100 μL of silver seeds, respectively.

To avoid changes in optical spectra over hours and days, all the samples were brought to boil for 3−4 min. The final concentration of silver for all the samples was kept at ca. 0.2 mM.

Lee−Meisel Silver Colloid. This colloid was synthesized according to the literature.[2] Typically, $AgNO_3$ (18 mg) was dissolved in 100 mL of H_2O and brought to boiling. A solution of 1% sodium citrate (2 mL) was added. The solution was kept on boiling for ca. 1 h. The Ag sols prepared by this procedure had an absorption maximum at about 420 nm.

SERS Experiments. A sample of 2-ATP (100 μL) prepared in ethanol solution was added to separate aliquots of silver colloid (2 mL) in a centrifugal tube, after shaking several times, and then allowed to stay for a half-hour to reach the adsorption equilibrium. Finally, various concentrations of NaCl were added to the above colloids to promote aggregation. FT-SERS measurements are performed by use of a quartz tube holding 300 μL of aggregated silver nanoplates. All the experiments were performed at room temperature (14 ± 2 °C).

Results and Discussion

Characterizations of Silver Nanoplates. Using seed-mediated growth approach, the size of the silver nanoplates can be controlled by adding an amount of small silver seeds. Larger nanoplates can be obtained using a smaller amount of silver seeds. Parts A−D of Figure 1 show the representative TEM images of these products. The dominant morphologies of them are thin nanoplates with various outlines, including truncated triangle, hexagon, and mild circlelike. A small percent of other shaped particles such as faceted silver nanospheres (~10%) can also be found. The size of the four samples (S1−S4), which were prepared using 2000, 700, 400, and 100 μL of silver seeds, is measured to be 45.5 ± 12.1, 63.0 ± 13.9, 80.2 ± 13.0, and 136.5 ± 17.1 nm, respectively. Figure 1E displays some nanoplates of sample S4 assembled into "stacks" on the TEM grids upon evaporation of solvent, which allow evaluation of their thickness (~14 nm). From the selected area electron diffraction (SAED) pattern (the inset of Figure 1D), each nanoplate can be identified to be a single-crystal bounded by {111} facets.[10d] The XRD pattern of these nanoplates (Figure 1E) further confirms this point.

The absorption spectra of all the as-prepared silver nanoplates display four peaks (Figure 2). A small and sharp peak at around

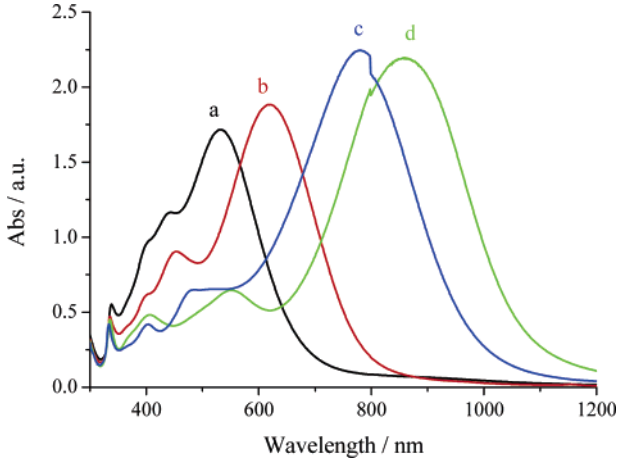

Figure 2. UV−vis absorption spectra of (a) sample S1, (b) sample S2, (c) sample S3, and (d) sample S4.

TABLE 1: Summary of Results for Silver Nanoplates

sample	nanoplate size[a] (nm)	SPR peaks (nm) λ_1	λ_2	λ_3	λ_4
S1	45.5 ± 12.1	338	401	440	530
S2	63.0 ± 13.9	335	397	450	619
S3	80.2 ± 13.0	334	402	477	778
S4	136.5 ± 12.1	336	406	550	858

335 nm is attributed to the out-of-plane quadrupole resonance of nanoplates. The second peak at 397−401 nm can be the contribution of some silver spherical particles, which had been indicated in the above TEM images. The third peak at 440−550 nm is attributed to the in-plane quadrupole resonance. The fourth peak at the longest wavelength side is due to the in-plane dipole resonance. This peak is closely correlated with the aspect ratio of silver nanoplates, which can be tuned by varying the amount of seeds. Through monitoring this peak by the UV−vis spectrophotometer, we purposely prepared four samples with the corresponding peak at 530, 619, 778, and 858 nm, respectively. Table 1 shows the summary results of these nanoplates.

UV−Vis Spectra and SERS Activity of Aggregated Silver Nanoplates. The correlations between the collective surface plasmon resonance and excitation wavelength reveal that higher SERS intensities can be achieved when the excitation wavelength is coincident with the wavelength of the absorption maximum of the aggregated excitation band.[12−15] While metal colloid UV−vis spectra are related to the surface plasmon resonance, whose frequencies depend on the aggregation pattern of the sol, they can be used to determine how the aggregation of silver nanoplates influences their optical properties.[16] In this way, we can choose suitable conditions for SERS measurements.

A small amount of 2-ATP added into the silver nanoplates can only slightly dampen the absorption maximum of silver nanoplates but is unable to result in the aggregation of them. The addition of a surplus of salt such as sodium chloride is necessary for the aggregation of silver nanoplates. The more the salt is added, the faster the aggregation rate of silver nanoplates is. A proper amount of salt is added into the colloids to make them moderately aggregate so as to facilitate recording the aggregated process of silver nanoplates by UV−vis spectrophotometer. Figure 3 shows the absorption spectra of all of these four samples after the addition of 2-ATP (100 μL, 1.0 × 10^{-4} M) and NaCl (20 μL, 2.0 M) to 2 mL of these colloids, as a function of increasing time, t = 0, 4, 8, 12, 16, 20, 24, 28, and 32 min. Among the four peaks of each sample, remarkable changes occur primarily on the fourth peak, whereas other peaks have small alterations in the site or intensity. As the aggregation proceeds, a new broad absorption band at the longest wavelength side appears and grows in the intensity at the expense of the in-plane dipole resonance of silver nanoplates. This band can be attributed to the coupling of the plasmon absorbance of the nanoplates, which are closely contacted. Recently, Gunnarsson et al. found that the dipolar surface plasmon resonance for incident polarization parallel to the axis of the pair of silver nanodisks red shifts dramatically when the interparticle distance is decreased, demonstrating that there were extremely strong interparticle interactions between silver nanodisks.[17] Because the in-plane dipole resonance of silver nanoplates is located in the lower energy region of the spectrum than the dipole resonance of common silver nanospheres (about 420 nm), the absorption maximum of aggregated silver nanoplates is more red-shifted than that of silver nanospheres (about 500−600 nm).[18] The strong absorption maximum of sample S1 has shifted to about 798 from 530 nm, and that of sample S2 has moved to about 920 from 619 nm, while that of sample S3 becomes broad with a shoulder band at about 1080 nm and that of sample S4 is considered to be over 1200 nm.

Parts a−d of Figure 4 show the corresponding FT-SERS spectra of 2-ATP on the aggregated silver nanoplates for different samples. The normal Raman spectrum of 2-ATP (0.5 M) in ethanol solution is shown for comparison in part f. The FT-SERS spectra show no significant changes in the spectral profile. However, the Raman intensity of samples S2−S4 are comparable, whereas that of sample S1 is the weakest since this sample has a small absorption at the excitation wavelength, as already shown in Figure 3a. The characteristic Raman vibration bands[19b,20] of 2-ATP such as ν(C−C) at 1472 cm^{-1}, δ(C−H) at 1030 cm^{-1}, and the ring-breathing mode at 845 cm^{-1} can be clearly seen in Figure 4a−d. In contrast, the SERS signal of unaggregated silver nanoplates is too weak to provide sufficient information about this probe molecule (Figure 4e), indicating that aggregation is essential for the SERS of 2-ATP to reach a detectable level. Previous theoretical and experimental studies showed that aggregates were more effective SERS systems than individual nanoparticles because large enhancement can be achieved at particles junctions of aggregates.[21−24] As calculated by Xu et al.,[21b] a large and spatially confined electromagnetic enhancement effect, on the order of 10^{11}, could be achieved for the case of strongly coupled structures, such as dimer configurations or sharp protrusions, while single spherical or nanocrystal shaped particles were found to produce a comparatively weak electromagnetic enhancement effect.

Comparison of SERS Activity of Aggregated Silver Nanospheres and Silver Nanoplates. In concordance with the Lee−Meisel silver colloids, we concentrated silver nanoplates from sample S4 to ca. 1.0 mM through the centrifugation (8000 rpm, 8 min) before SERS measurements. Figure 5 shows the SERS spectra of 2-ATP (5.0 × 10^{-6} M) adsorbed on silver nanoplates and silver nanospheres. The concentration of sodium chloride in the suspensions used for measurement is 40 mM. The FT-SERS spectra of them are very similar, except for changes in Raman intensity. But silver nanoplates have stronger SERS activity than silver nanospheres. For example, the Raman intensity of the ν(C−C) mode at 1472 cm^{-1} from nanoplates is ca. 11 times stronger than that of Lee−Meisel colloids. In the studies of the SERS effect of silver nanoparticles with different shapes, Zhang et al.[25] found that the Raman enhancement of silver nanospheres was better than that of silver nanowires and silver nanoplates, and silver nanoplates were the worst, and they

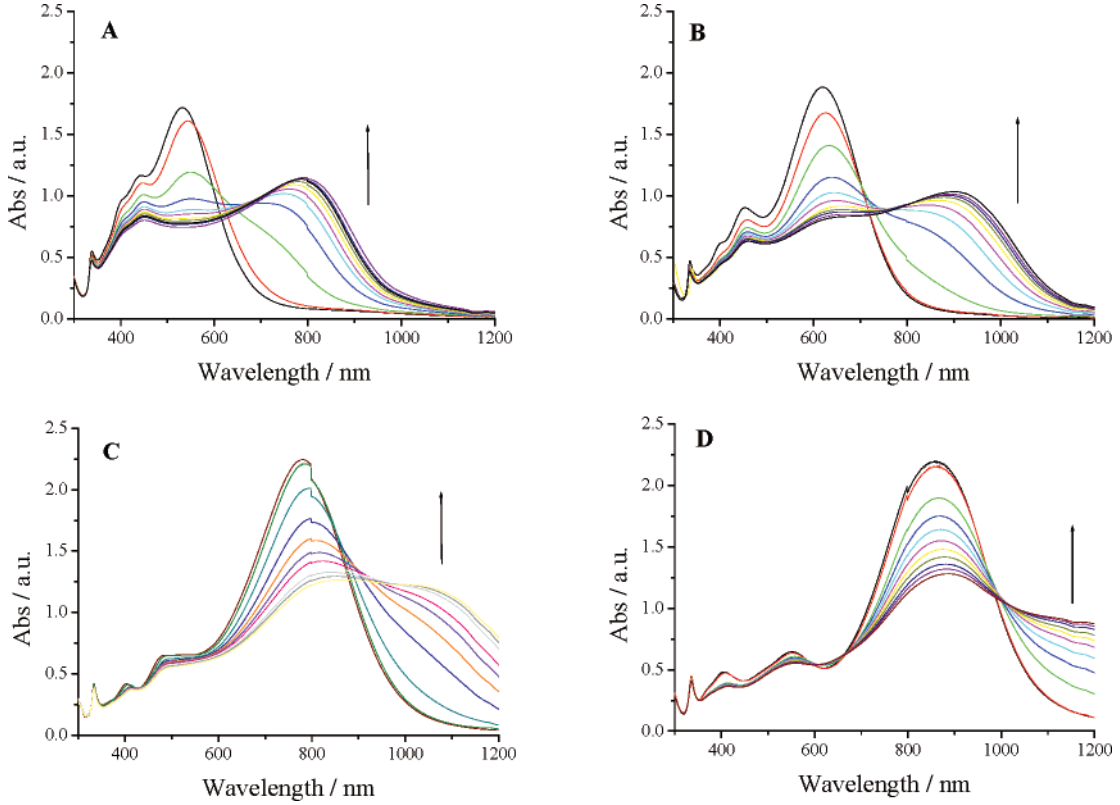

Figure 3. UV−vis absorption spectra of (A) sample S1, (B) sample S2, (C) sample S3, and (D) sample S4, after the addition of 2-ATP (100 μL, 1.0×10^{-4} M) and NaCl (20 μL, 2.0 M) to 2 mL of these colloids, as a function of increasing time, $t = 0$, 4, 8, 12, 16, 20, 24, 28, and 32 min.

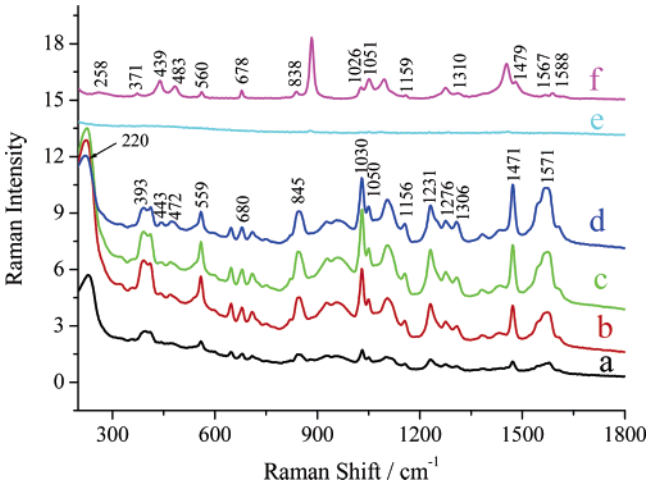

Figure 4. FT-SERS spectra of 2-ATP (5×10^{-6} M) adsorbed on aggregated nanoplates from (a) sample S1, (b) sample S2, (c) sample S3, and (d) sample S4. 2-ATP (100 μL, 1.0×10^{-4} M) was added into 2 mL of silver nanoplate solution, and NaCl (20 μL, 2.0 M) was used to promote aggregation. (e) FT-SERS spectra of 2-ATP (5×10^{-6} M) adsorbed on unaggregated silver nanoplates from sample S4 (without additional salt). (f) Normal Raman spectrum of 2-ATP (0.5 M) in ethanol solution for comparison.

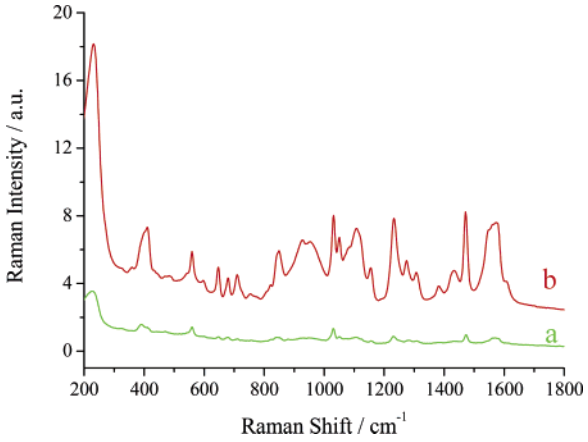

Figure 5. Comparison of the SERS activity of 2-ATP (5×10^{-6} M) adsorbed on (a) aggregated Lee−Meisel colloids, and (b) aggregated nanoplates from sample S4. 2-ATP (100 μL, 1.0×10^{-4} M) was first added into 2 mL of the above colloidal solutions, and NaCl (40 μL, 2.0 M) was used to promote aggregation.

concluded that the crystal planes had great effect (chemical effect) on Raman enhancement of rhodamine B at these silver colloids. Because their experimental procedures and conditions are different from ours, it is difficult to make direct comparisons with theirs. But it should be pointed out that the area ratio of edges/basal planes, i.e., the ratio of higher energy planes/(111) crystal planes, for silver nanoplates, could not be negligible in some cases. On the basis orf the thickness (D) and diameter (R) parameters of silver nanoplates from sample S4, we can roughly estimate the area ratio of edges/basal planes to be close to $3D/R \sim 2D/R = 31\% \sim 21\%$, provided that all the particles are either perfect silver nanoprisms or nanodisks. For smaller silver nanoplates, this value is expected to be higher than that of large ones. In this regard, it seems that the crystal planes with higher surface energies in silver nanoplates are not inferior to those in silver nanospheres. As shown previously in many reports on SERS,[25−31] the SERS enhancement is the result of a combination of electromagnetic effect and chemical effect, but chemical effect is generally thought to contribute only a factor of $10-10^2$, compared to factors of 10^4-10^7 for electromagnetic effect.[30] In the present study, the SERS enhancement of our samples must also come from both electromagnetic effect and chemical effect. The chemical effect involved in the SERS process is supported by the facts that the δ(C−S) bending mode

at 371 cm^{-1} and ν(C−S) stretching mode at 483 cm^{-1} in the normal Raman spectrum of pure 2-ATP have been shifted to 411 and 470 cm^{-1}, respectively, in the SERS spectra of adsorbed 2-ATP (Figure 5b). But electromagnetic effect arising from the coupling silver nanoplates is believed to produce the dominant contribution to the SERS activity of silver nanoplates. As mentioned above, aggregation is essential for the SERS of 2-ATP to reach a detectable level. In addition, selecting the excitation wavelength is also very important for obtaining higher SERS activity. Under the off-surface plasmon resonance condition (relative to the new band of aggregated silver nanoplates), such as using 514 nm as the exciting laser source, no interpretable SERS signal can be obtained for all the samples. Because enhanced local fields are associated with the excitation wavelength[13−16] and higher curvature features on the surface,[31,32] it is considered that the better SERS performance of silver nanoplates relative to silver nanospheres is closely related with the red shift of SPR peaks, as well as the corners and edges of silver nanoplates.

Estimation of Enhanced Factor of Silver Nanoplates. To quantitatively evaluate the magnitude of the enhancement factor (EF) for silver nanoplates, we compare the measured SERS intensities to the intensity of nonenhanced Raman scattering by using the following equation:[18]

$$\mathrm{EF} = (I_{\mathrm{SERS}}/C_{\mathrm{SERS}})/(I_{\mathrm{normal}}/C_{\mathrm{bulk}})$$

where C_{bulk} is the concentration of the molecules in the bulk samples, C_{SERS} is the concentration of the adsorbed molecules on the silver surface; I_{normal} and I_{SERS} are the intensity of a certain vibration in normal and SERS Raman spectra, respectively. The enhancement factor is obtained by comparing the SERS spectrum of 2-ATP adsorbed on silver nanoplates (take sample S4, for example) with normal Raman spectrum of pure 2-ATP (0.5 M) in ethanol solution. I_{normal} and I_{SERS} are measured at 1030 cm^{-1}. Actually, 5.0×10^{-6} M of 2-ATP used in this study is very close to the concentration of a monolayer of 2-ATP adsorbed on the silver surface. Using the thickness and diameter parameters of silver nanoplates, we can likewise estimate the number of the surface atoms of silver nanoplates (denoted as the concentration unit) and so the concentration of a monolayer of 2-ATP adsorbed on the silver surface. The diameter of an Ag atom is calculated from the relation $d = (V_{\mathrm{m}}/(6.03 \times 10^{23}))^{1/3}$ (V_{m} =10.5 mL/mol, molar volume of silver);[33,34] i.e., $d = 0.259$ nm. The concentration of silver nanoplates is 0.2 mM. Imagining that all the silver nanoplates in the solution are arranged in an edge-to-edge manner into one huge nanoplate, and assuming that this huge nanoplate is compactly piled up by a plane composed of single silver atom layer, there should be about 54 layers of such planes for a nanoplate with a thickness of 14 nm. So the concentration of silver for one such plane should be 3.7×10^{-6} M, which is equal to the concentration of the surface atoms of one basal planes. Taking into account the edges of silver nanoplates (about 21−31% of the basal plane), the total concentration of the silver surface atom should be about $(9.0-9.7) \times 10^{-6}$ M. The van der Waals dimensions of 2-ATP are assumed to be 4 Å × 7 Å (equal to the area of four silver atoms arranged in a plane).[19] Therefore, about $(2.3-2.4) \times 10^{-6}$ M of 2-ATP is required for a monolayer of these molecules formed on the silver surface. We calculated the enhancement factor for 5.0×10^{-6} M of 2-ATP adsorbed on the aggregated silver nanoplates to be $\sim 4.5 \times 10^5$. Values of similar magnitude have been observed on other SERS-active silver substrates.[35,36]

Conclusions

Traditionally, it is thought that the coupling of the particles upon aggregation in aqueous solution may take place normally on these more isotropic particles such as nanospheres or ellipsoids, but we have demonstrated that highly anisotropic silver nanoplates could also be coupled with each other upon aggregation in aqueous solution. Although a more complicated configuration in aggregated forms of silver nanoplates is expected than that of silver nanospheres, e.g., face to face, edge to edge, or edge to face, our results showed large Raman enhancement in the case of aggregation. Using 2-ATP as probing molecules, an enhancement factor of 4.5×10^5 can be obtained for aggregated silver nanoplates in aqueous solution. This large enhancement is believed to mainly come from electromagnetic effect through the interacting silver nanoplates. Since the new plasmon resonance of aggregated silver nanoplates in aqueous solution is more red-shifted than that of the commonly used Lee−Meisel silver colloids, they are a very desirable substrate for near-IR Raman measurements. In addition, as the strong SPR of an individual silver nanoplate can be tunable in a broad range from the visible to near-IR region, these particles are expected to have other potential uss, such as detecting biomolecules by surface-enhanced resonance Raman scattering.

Acknowledgment. This work was supported by the National Natural Science Foundation of China (Grant Nos. 20575064 and 20427003).

References and Notes

(1) Chang, R. K.; Furtak, T. E. *Surface Enhanced Raman Scattering*; Plenum Press: New York, 1982.
(2) Lee, P. C.; Meisel, D. *J. Phys. Chem.* **1982**, *86*, 3391.
(3) Munro, C. H.; Smith, W. E.; Garner, M.; Clarkson, J.; White, P. C. *Langmuir* **1995**, *11*, 3712.
(4) L. Rivas, Sanchez-Cortes, S.; Garcia-Ramos, J. V.; Morcillo, G. *Langmuir* **2001**, *17*, 574.
(5) Creighton, J. A.; Blatchford, C. G.; Albrecht, M. G. *J. Chem. Soc., Faraday Trans. 2* **1979**, *75*, 790.
(6) Nikel, U.; Castell, A.; Poppl, K.; Schneider, S. *Langmuir* **2000**, *16*, 9087.
(7) Leopold, N.; Lendl, B. *J. Phys. Chem. B* **2003**, *107*, 5723.
(8) Canamares, M. V.; Garcia-Ramos, J. D.; Gomez-Varga, J. D.; Domingo, C.; Sanchez-Cortes, S. *Langmuir* **2005**, *21*, 8546.
(9) Li, Y.; Cheng, J.; Coons, L. B. *Spectrochim. Acta, Part A* **1999**, *55*, 1197.
(10) (a)Jin, R.; Cao, Y.; Mirkin, C. A.; Kelly, K. L.; Schatz, G. C.; Zheng, J. G. *Science* **2001**, *294*, 1901. (b) Callegari, A.; Tonti, D.; Chergui, M. *Nano Lett.* **2003**, *3*, 1565. (c) Maillard, M.; Huang, P.; Brus, L. *Nano Lett.* **2003**, *3*, 1611. (d) Sun, Y.; Xia, Y. *Adv. Mater.* **2003**, *15*, 9. (e) Sun, Y.; Mayers, B.; Xia, Y. *Nano Lett.* **2003**, *3*, 675.
(11) (a) He, Y.; Shi, G. *J. Phys. Chem. B* **2005**, *109*, 17503.(b) Brioude, A.; Pileni, M. P. *J. Phys. Chem. B* **2005**, *109*, 23371.
(12) Li, X.; Xu, W.; Zhang, J.; Jia, H.; Yang, B.; Zhao, B.; Li, B.; Ozaki, Y. *Langmuir* **2004**, *20*, 1298.
(13) Siiman, O.; Bumm, L.; Callaghan, R.; Blatchford, C. G.; Kerker, M. *J. Phys. Chem. B* **1983**, *87*, 1014.
(14) Gersten, J. I.; Nitzan, A. *Surf. Sci.* **1985**, *158*, 165.
(15) Olson, L.; Lo, Y.; Beebe, T.; Harris, J. *Anal. Chem.* **2001**, *73*, 4268.
(16) Felidj, N.; Levi, G.; Pantigny, J.; Aubard, J. *New J. Chem.* **1998**, 725.
(17) Gunnarsson, L.; Rindzevicius, T.; Prikulis, J.; Kasemo, B.; Kall, M.; Zou, S.; Schatz, G. *J. Phys. Chem. B* **2005**, *109*, 1079.
(18) Rivas, L.; Sanchez-Cortes, S.; Garcia-Ramos, J. V.; Morcillo, G. *Langmuir* **2000**, *16*, 9722.
(19) (a) Nikoobakht, B.; Wang, J.; EI−Sayed, M. *Chem. Phys. Lett.* **2002**, *366*, 17. (b) Nikoobakht, B.; EI−Sayed, M. A. *J. Phys. Chem. A* **2003**, *107*, 3372.
(20) Griffith, W.; Koh, T. *Spectrochim. Acta* **1995**, *51*, 253.
(21) (a) Xu, H.; Bjerneld, E. J.; Kall, M.; Borjesson, L. *Phys. Rev. Lett.* **1999**, *83*, 4357. (b) Xu, H.; Aizpurua, J.; Kall, M.; Apell, P. *Phys. Rev. Lett.* **2000**, *62*, 4318.
(22) (a) Bosnick, K.; Jiang, J.; Brus, L. *J. Phys. Chem. B* **2002**, *106*, 8096. (b) Jiang, J.; Bosnick, K.; Maillard, M.; Brus, L. *J. Phys. Chem. B* **2003**, *107*, 9964.

(23) Futamata, M.; Maruyama, Y.; Ishikawa, M. *J. Phys. Chem. B* **2004**, *108*, 13119.
(24) Schwartzberg, A.; Grant, C.; Wolcott, A.; Talley, C.; Huser, T.; Bogomolni, R.; Zhang, J. *J. Phys. Chem. B* **2004**, *108*, 19191.
(25) Zhang, J.; Li, X.; Sun, X.; Li, Y. *J. Phys. Chem. B* **2005**, *109*, 12544.
(26) Hildbrandt, P.; Stockburger, M. *J. Phys. Chem.* **1984**, *88*, 5935.
(27) Osawa, M.; Matsuda, N.; Yoshii, K.; Uchida, I. *J. Phys. Chem.* **1994**, *98*, 12702.
(28) Yu, H.; Zhang, J.; Zhang, H.; Liu, Z. *J. Phys. Chem.* **1911**, *15*, 16.
(29) Doering, W.; Nie, S. *J. Phys. Chem. B* **2002**, *106*, 311.
(30) Campion, A.; Kambhampati, P. *Chem. Soc. Rev.* **1998**, *27*, 241.
(31) Schatz, G. C. *Acc. Chem. Res.* **1984**, *17*, 370.
(32) Hao, E.; Bailey, R.; Schatz, G. C.; Hupp, J.; Li, S. *Nano Lett.* **2004**, *4*, 327.
(33) Henglein, A.; Giersig, M. *J. Phys. Chem. B* 1999, *103*, 9533.
(34) Michaelis, M.; Henglein, A.; Mulvaney, P. *J. Phys. Chem. B* **1994**, *98*, 6212.
(35) Ibrahim, A.; Oldham, P.; Stokes, D.; Vo-Dinh, T. *J. Raman. Spectrosc.* **1996**, *27*, 887.
(36) Tao, A.; Kim, F.; Hess, C.; Goldberger, J.; He, R.; Sun, Y.; Xia, Y.; Yang, P. *Nano Lett.* **2003**, *3*, 1229.